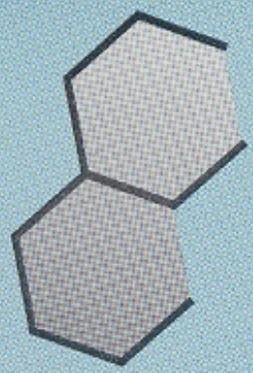

Carbon'02 in Beijing

An International Conference on Carbon
15-19 September 2002 Beijing, CHINA

SHANXI CHUNQIU AUDIO-VISUAL PRESS
ISBN 7-900362-03-7/G.03

CARBON '02

An International Conference on Carbon

September 15-20, 2002 Beijing, China

ASYMMETRICAL RELAXATION OF CONDUCTION ELECTRON SPINS AT COLLISIONS WITH THE FRONT OF GRAPHITE INTERCALATION BY SbF_5

A.M. Ziatdinov* and A.G. Sviridova

Institute of Chemistry, Far Eastern Branch of the Russian Academy of Sciences.
159, Prosp. 100-letiya, 690022 Vladivostok, Russia.

Abstract – Results of an *in situ* conduction ESR (CESR) study of SbF_5 molecules intercalation into highly oriented pyrolitic graphite are presented. The narrowing (broadening) of the CESR signal from the intercalated (the non-intercalated) parts of the graphite plate during the advance of the reaction front into graphite is explained by the non-zero probability of the spin reorientation at the collisions of current carriers with the intercalation front and by the decrease (increase) of the frequency of these collisions. The assumption was made that the reasons for step-wise increasing in the intensity of CESR signal from the intercalated parts of graphite plate during the reaction are presence of the threshold intercalation potential and periodical impoverishing of the adsorbed layers of intercalate.

Keywords: **A**. intercalation compounds; **B**. electron paramagnetic resonance; **D**. electronic and magnetic properties.

1. INTRODUCTION

In recent years, solid state physicists have been attracted in growing number of the study of intercalation compounds and diffusion processes in these materials [1-6]. This interest is largely derived from the extensive diversity of phenomena and fundamental new physics exhibited by these compounds. There is also the possibility of practical applications such as their use as very efficient catalysts, as electrodes in high energy density batteries, and the synthesis of light high-conductivity materials.

Graphite intercalation compounds (GICs) form one of the largest family of the intercalation compounds. The intercalation process and staging phenomena in GICs are in focus of attention of the researchers during the long time [1-6]. But up to now, in spite of numerous publications devoted to studies of various aspects of GICs structure and properties, many aspects of mechanism of "guest" molecule intercalation into graphite have not received sufficient attention. ë

The conduction ESR (CESR) technique is one of the most powerful methods for studying the graphite intercalation process, because shapes and intensities of the CESR signal both from non-intercalated and intercalated regions of graphite plate vary strongly during the intercalation. However, because of the difficulty of such experiments only a few CESR studies of graphite intercalation process have been undertaken [7-13]. But even in these cases, because of presence of the skin effect, the interpretation of changes in the graphite CESR signal during the intercalation process is not trivial.

This paper is devoted to the results of in situ CESR study of antimony pentafluoride (SbF_5) molecule intercalation into highly oriented pyrolitic graphite (HOPG) plates with width being 1) comparable and 2) much more than the skin-depth, δ_c, governed by the magnetic component of the microwave field (Fig. 1). The obtained experimental results clearly show the stepwise ***c***-axis conductivity σ_c. The experiments were carried out for two different orientations of the ***c***-axis relative to the nature of the intercalation process and the large asymmetrical spin relaxation probability at collisions of current carriers with the graphite intercalation front.

*Corresponding author. Fax: +7-4232-311889; e-mail address: albert_ziatdinov@mail.primorye.ru

2. EXPERIMENTAL

CESR measurements were carried out at room temperature using an X-band E-line spectrometer in a rectangular cavity with TE_{102} mode. The constant magnetic field, H_0, modulation frequency and amplitude were 2.5 kHz and 0.1 mT, respectively.

The HOPG samples investigated were in the shape of rectangular parallelepipeds with the dimensions: height (h)×width (l)×thickness (d), where $h \times l$ is the area of the basal plane and on samples in the shape of disks with the dimentions: diameter (D)×thickness (d), where $\pi D^2/4$ is the area of the basal plane. The rectangular HOPG plates with dimensions: 0.94×0.58×0.035 cm^3 (sample A) and 0.4×0.032×0.034 cm^3 (sample B) and the HOPG disk with D=0.27 cm and d=0.014 cm (sample C) were used in ESR-measurements. The measurements of the basal plane conductivity, σ_a, of the (HOPG+SbF_5) system were carried out on A type graphite sample.

The EPR-experiments were carried out both in a traditional configuration of such experiments - with the basal $l \times h$ and lateral $d \times h$ sides of the rectangular plates were parallel and the ***c***-axis was perpendicular to the Z-axis of the cavity (Fig. 1a), and in nontraditional configuration of such experiments - with the basal planes of plate were perpendicular and the ***c***-axis was parallel to the to the Z-axis of the cavity (Figs. 1b and 1c). Note, that in the rectangular resonator, the structure of electromagnetic field of TE_{102} mode has such a form that, at a conventional setting of the resonator, $\boldsymbol{H}_0$ is parallel to the electrical component, $\boldsymbol{E}_{rf}$, of microwave field (Fig. 1).

The HOPG samples were held in quartz tube connected via a valve to the reservoir with intercalate (liquid SbF_5 with the vapour pressure ~1 Torr). The SbF_5 vapour penetrated into the knee of reactor with the graphite

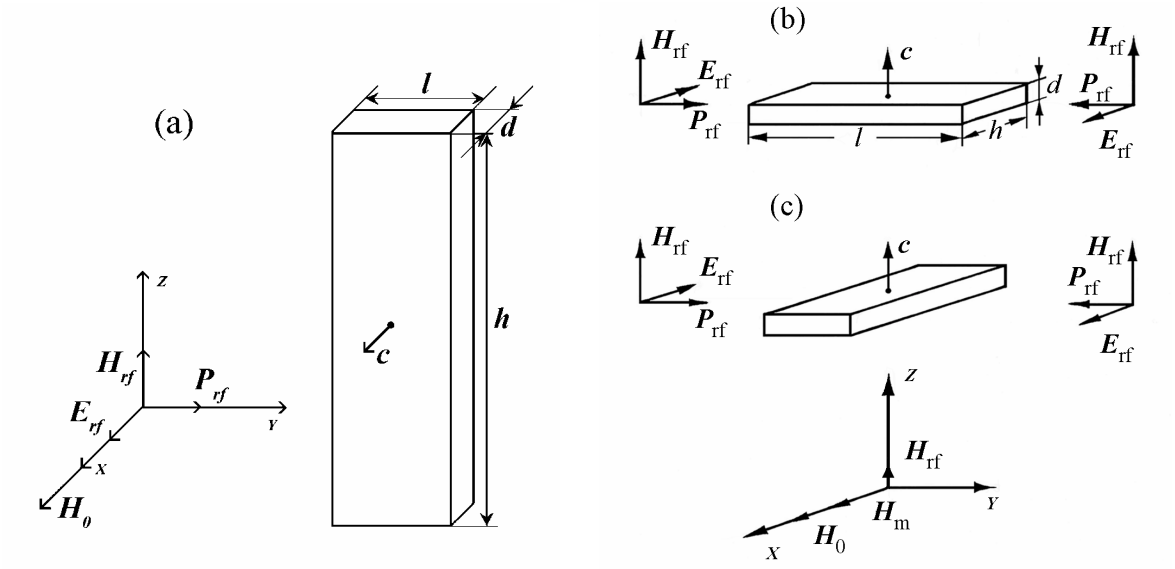

Fig. 1. Orientation of the vectors of the external static magnetic field $\boldsymbol{H}_0$, the modulating magnetic field $\boldsymbol{H}_m$, the electric field $\boldsymbol{E}_{rf}$ and magnetic field $\boldsymbol{H}_{rf}$ components of the microwave field, and the Poynting vector $\boldsymbol{P}_{rf}$ in unloaded rectangular cavity relative to a graphite plate with the geometric dimensions width (l)×height (h)×thickness (d). The left and right figures refer, respectively, to $\boldsymbol{H}_{rf}$ perpendicular and parallel to the $\boldsymbol{c}$-axis.

sample through the hole with the size ~5×10^{-2} cm^2 in the fluoroplastic diaphragm. Prior to the experiment, the system was evacuated to eliminate air and water.

In situ measurements of the σ_a for the (HOPG+SbF_5) system were carried out by the contactless Wien bridge method being analogous to that described in ref. [14]. According to data of the four-probe method, at 300 K the σ_c for HOPG plate used is equal to (7.7±0.8) S/cm. In the X- band ESR-experiment the value of the skin depth δ_c~0.02 cm corresponds to this conductivity, i. e. in experiments of graphite intercalation by SbF_5 the whole volume of the sample B was available for the CESR studies.

3. RESULTS

The CESR spectrum of all HOPG plates investigated consists of a single asymmetric line determined by the Dyson-Kaplan mechanism [15, 16]. The spectrum is axial with respect to the $\boldsymbol{c}$-axis and the principal values of g-factor determined by Feher-Kip [17] nomograms or those of Kodera [18] are equal to g_c=2.0474±0.0002 and g_a=2.0029±0.0002 for $\boldsymbol{H}_0\|\boldsymbol{c}$ and $\boldsymbol{H}_0\perp\boldsymbol{c}$, respectively. The lineshape asymmetry parameter, A/B, being determined as the maximum-to-minimum peak height ratio, both measured with respect to the base line of the first derivative of CESR absorption line, is 'normal' in the sense that the greater peak, A, occurs at the lower magnetic fields, than the smaller peak B, and it is equal to ≅4 for sample A and ≅2.3 for sample B. I. e. in sample with $l >> \delta_c$ the value of A/B is essentially 'metallic'. Small value of A/B for the graphite plate with $l \cong 1.6\delta_c$ is caused by the fact that CESR lineshape tends to Lorentzian with A/B=1 at $l\to0$.

In certain time (so-called "induction" time of the reaction which depends on sample size and experimental conditions) after the injection of SbF_5 gas into the knee of the reactor with the HOPG plate, the CESR signal of graphite begins to transform and decrease in intensity until it fully disappears (Fig. 2 and 4). Simultaneously a new signal with g_c*=2.0025±0.0002, and g_a*=2.0028±0.0002 appears in the spectrum (Fig. 3 and 4), where g_i* (i=a, c) value is determined by the $\boldsymbol{H}_0$ value at the point of intersection of the first derivative of CESR absorption line and the base line.

In sample A at the moment of first observation the value of the asymmetry parameter, A^*/B^*, of CESR signal with g_i* is ~1, then it monotonously increases up to ~1.6 to the end of reaction (Fig. 3). In sample B at the moment of first observation the A^*/B^* value is also near 1, but further it increases and forms a peak with the maximal value of A^*/B^* ~ 3, and then decreases up to the value ~1.7 to the end of reaction. In both samples investigated the linewidth, ΔH^*, of CESR signal with g_i* monotonously decreases in several times to the end of reaction (Fig. 3). The g_i*-values of this signal remain constant up to the end of intercalation. In samples A and C for any orientation of the $\boldsymbol{c}$-axis relative to the cavity axis the dependence of intensity, $I^*=(A^*+B^*)\times\Delta H^{*2}$, of CESR signal with g_i* on exposure time, τ, take a well-marked step-wise form (Fig. 4 and 5). In sample B such stepwise increase of intensity of CESR signal with g_i* was not revealed.

In a traditional configuration of the EPR experiment in both samples A and B the linewidth (the intensity), ΔH ($I=(A+B)\times\Delta H^2$), of the graphite CESR signal increases (decreases) versus exposure time monotonously (Fig. 2, 4 and 6). In sample A at the beginning of reaction the A/B ratio of graphite signal increases, but it is still 'normal' reaching a maximum value of A/B ~12. Later, upon further exposure in the intercalate atmosphere, the A/B ratio becomes 'reversed' (maximum peak height, A, occurs at the higher magnetic fields than the peak B), and its magnitude decreases down to value ~5; the A/B maximum corresponds to the moment when the 'reversal' of CESR lineshape takes place (Fig. 2). The g_i

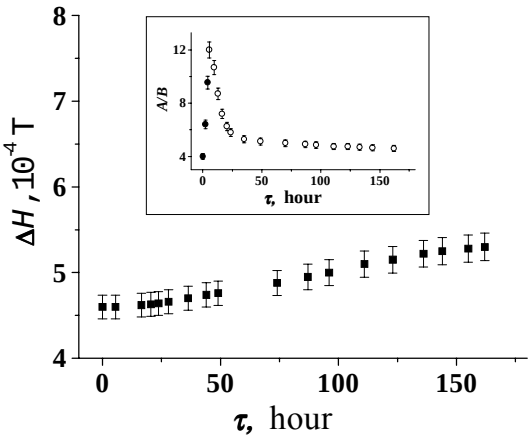

Fig. 2. CESR lineshape parameters of unintercalated parts of HOPG plate (sample A) versus exposure time, τ, in SbF_5 atmosphere. In insert, the shaded and open dots are referred to the normal and 'reversed' lineshape, respectively; half-shaded dot corresponds to the lineshape with symmetric phase with respect to the *A* peak. The X-band; T=300 K; $\boldsymbol{c} \parallel \boldsymbol{H}_0, \perp [\boldsymbol{E}_{rf} \times \boldsymbol{H}_{rf}]$.

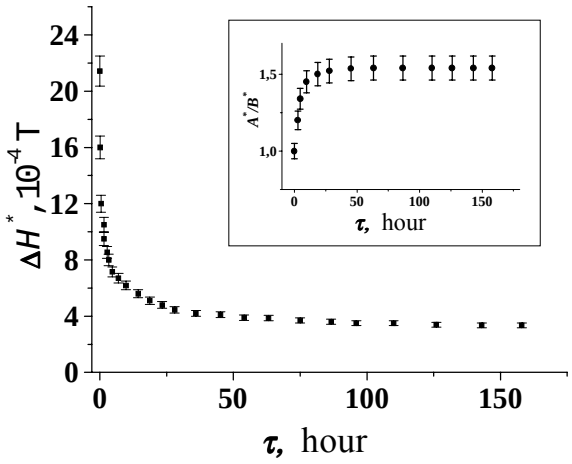

Fig. 3. CESR lineshape parameters of intercalated parts of HOPG plate (sample A) versus exposure time, τ, in SbF_5 atmosphere. The X-band; T=300 K; $\boldsymbol{c} \parallel \boldsymbol{H}_0, \perp [\boldsymbol{E}_{rf} \times \boldsymbol{H}_{rf}]$.

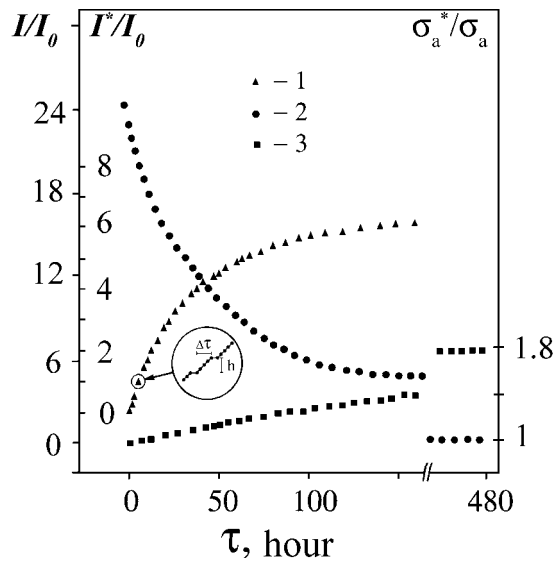

Fig. 4. The ratio of intensities of CESR signal from unintercalated, I/I_0, and intercalated, I^*/I_0, parts and σ_a^*/σ_a - conductivity of HOPG plate (sample A) versus exposure time, τ, in SbF_5 atmosphere. 1, 2 and 3 correspond to I^*/I_0, I/I_0 and σ_a^*/σ_a, respectively; $I^*=(A^*+B^*)\times(\Delta H^*)^2$; I_0 is the intensity of the Mn^{2+} ESR signal in a standart sample ($ZnS:Mn^{2+}$). The X-band; T=300 K; $\boldsymbol{c} \parallel \boldsymbol{H}_0, \perp [\boldsymbol{E}_{rf} \times \boldsymbol{H}_{rf}]$.

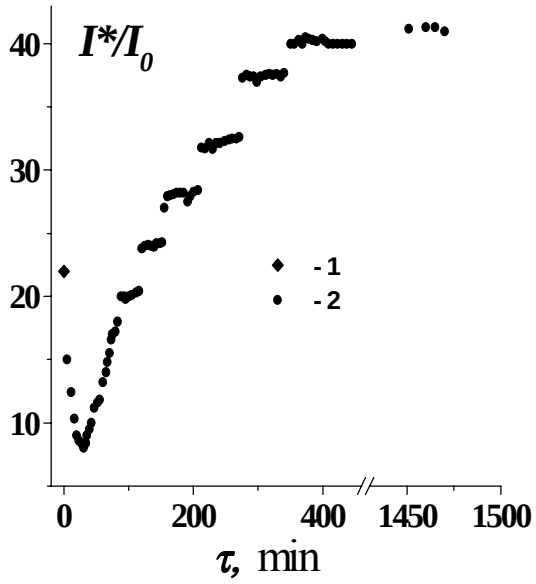

Fig. 5. The ratio of intensities, I^*/I_0 (2), of CESR signal from intercalated parts of HOPG plate (sample A) versus exposure time, τ, in SbF_5 atmosphere. The point 1 corresponds to the intensity, I/I_0, of CESR from initial HOPG plate. $I^*=(A^*+B^*)\times(\Delta H^*)^2$; $I=(A+B)\times\Delta H^2$; I_0 is the intensity of the Mn^{2+} ESR signal in a standart sample ($ZnS:Mn^{2+}$). The X-band; T=300 K; $\boldsymbol{c} \perp \boldsymbol{H}_0, \parallel [\boldsymbol{E}_{rf} \times \boldsymbol{H}_{rf}]$.

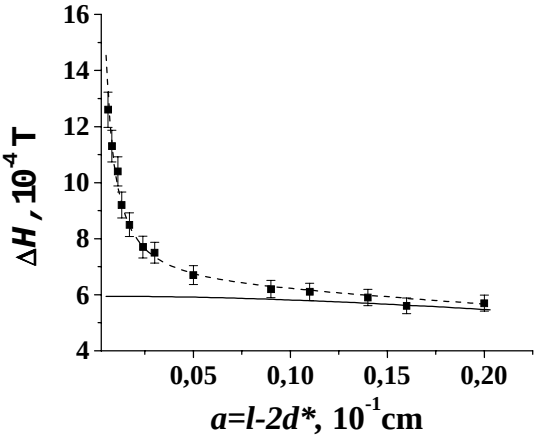

Fig. 6. The experimental (dots) and theoretical (lines) values of CESR linewidth, ΔH, versus thickness, $a=l-2d^*$, of the nonintercalated (by SbF_5) part of HOPG plate (sample B). The dashed line: G_a= 1 cm^{-1}, T_2=1.16×10^{-8} s, R_a=2.35, δ_c=0.02 cm; the solid line: G_a=0 cm^{-1}, T_2=1.16×10^{-8} s, R_a=2.35, δ_c=0.02 cm. T=300 K; $\boldsymbol{c} \parallel \boldsymbol{H}_0, \perp [\boldsymbol{E}_{rf} \times \boldsymbol{H}_{rf}]$.

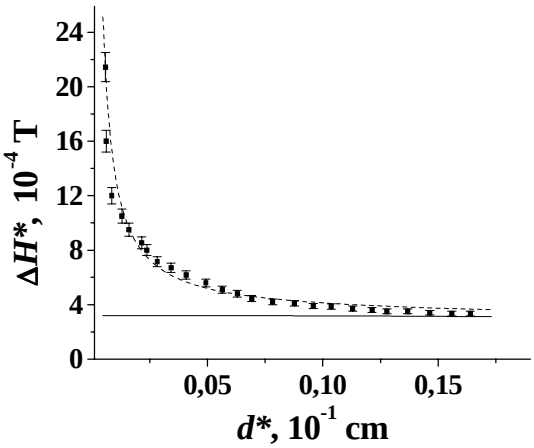

Fig. 7. The experimental (dots) and theoretical (lines) values of CESR linewidth, ΔH^*, versus thickness, d^*, of the intercalated (by SbF_5) part of HOPG plate (sample A). The dashed line: G_a=0.3 cm^{-1}, T_2=2.3×10^{-8} s, δ_c=0.03 cm, R_a=0.5; the solid line: G_a=0 cm^{-1}, T_2=2.3×10^{-8} s, δ_c=0.03 cm; R_a=0.5. T=300 K; $\boldsymbol{c} \parallel \boldsymbol{H}_0, \perp [\boldsymbol{E}_{rf} \times \boldsymbol{H}_{rf}]$.

(i=a, c) value of graphite CESR signal does not change up to its disappearance. It is important to note that in the sample B the character of the graphite CESR lineshape evolution is similar to that observed in sample A, but in this sample to the moment of graphite CESR signal disappearance the value of linewidth is much more than in the sample A at the corresponding time of reaction (Figs. 2 and 6).

4. DISCUSSION

In a traditional configuration of ESR-experiment (Fig. 1a) the microwave field penetrates into the HOPG plate mainly through its lateral sides, which are parallel to both the c-axis and $\boldsymbol{H}_{rf}$ and perpendicular to the $\boldsymbol{P}_{rf}$ [19], i.e. through the lateral sides $h \times d$. Therefore, the evolution of graphite CESR signal of the samples investigated (Figs. 2- 4 and 6) is mainly due to variations of the composition and properties of the HOPG plate at the surface areas with the thickness near δ_c from these sides. The dependence of the shape and intensity of graphite CESR signal on exposure time of a sample in SbF_5 vapours is qualitatively identical to that of the ESR signal lineshape and intensity of the localized spins in a metallic substrate on the thickness of a spray-coated film of another metal [20]. In our case, the spins in consideration are certainly mobile, but for $l/\delta_c<2$ the CESR line shape does not depend on spin mobility (Fig. 8), i. e., in the framework of the Dyson theory [15] in sample B the spin carriers may be considered as localized. Therefore, the variations of the shape and intensity of the graphite CESR signal of the sample B (Figs. 6) may be considered as being due to the formation of a macroscopic 'intercalation' layer on the HOPG plate (with conductivity being different from that of the initial material) and by advance of the interface separating this layer from as-yet the non-intercalated parts of sample (due to the diffusion of nitric acid molecules into the substrate along the graphite galleries). With the account that in samples A and B the CESR signal lineshape and intensity variations are qualitatively identical it is possible to assume that they have the same origin also. In a nontraditional configuration of ESR-experiment (Fig. 1, b and c) the microwave field penetrates into the HOPG plate mainly through its lateral sides $h \times d$ (the configuration 1b) and $h \times l$ (the configuration 1c), which are parallel to both the c-axis and $\boldsymbol{H}_{rf}$ and variations of the composition and properties of the HOPG perpendicular to the $\boldsymbol{P}_{rf}$. Therefore, the evolution of CESR signal of the sample A (Fig. 5) may be considered as due to plate at the surface areas with the thickness near δ_a from these sides.

The invariability of the g-factor values for CESR signal from HOPG substrate (g_i) and that from 'intercalation' layer (g_i^*) up to the disappearance of signal and the end of reaction, respectively, indicates that the interface between 'intercalation' layer and as-yet the non-intercalated parts of sample may be considered as non-conductive. The non-conductivity of this interface may be caused by significant distortion of a carbon net near the intercalation front and/or by the presence of high phase-boundary electrostatic potential due to the different current carriers concentration in the intercalated parts of graphite and in the non-intercalated ones.

In the experiments with sample B, the whole volume of sample investigated is available for CESR studies. Therefore, the time of the graphite CESR signal disappearance corresponds approximately to the moment of contact of the counter (antiparallel) intercalation fronts. Let us assume, that the intercalation is determined by a two-dimensional diffusion-controlled process, i.e. the thickness of the intercalated layer, d^*, depends on the intercalation time, $\Delta\tau$, as $(d^*)^2=2D_{int} \times \Delta\tau$, where D_{int} is intercalate two-dimensional diffusion constant. In such a case, having substituted the value of time interval from the beginning of the graphite CESR signal transformation up to its disappearance (Fig. 2) and $d^*=1/2$ to this expression, it is easy to estimate the value $D_{int} \sim 2.4 \times 10^{-14}$ m^2 s^{-1}.

A new and unexpected result of our experiments are the significant broadening of the graphite CESR signal from the beginning of the intercalation up to the contact of the counter intercalation fronts (Figs. 6) and significant narrowing of the CESR signal from the intercalated parts of the graphite plate at the beginning of intercalation (Figs. 3). We suppose that reason both these unusual lineshape dependencies are the collisions of current carriers (at their diffusion along the graphite layers) with the non-conductive interface between the intercalated and the non-intercalated parts of the HOPG plate. Indeed, when the intercalation front advances into the plate (due to the diffusion of nitric acid molecules into the graphite along the graphite galleries) the width of its non- intercalated part decreases and, therefore, the frequency of collisions of graphite current carriers with these interfaces increases. Therefore, assuming the probability of spin reorientation of graphite current carriers during such collisions to be non-zero, the increase of the total rate of spin relaxation of graphite current carriers (the graphite CESR linewidth) with the time of intercalation can be observed.

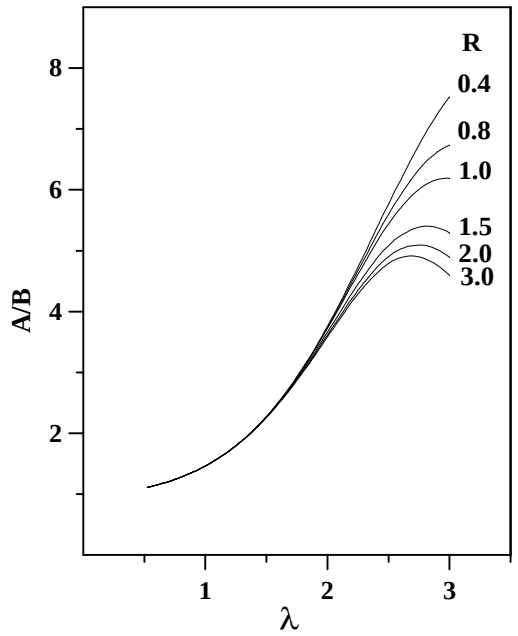

Fig. 8. The asymmetry parameter of the first derivative of CESR absorption line, A/B, vs. the $\lambda=L/\delta$ (L is the sample size, δ is the skin-depth). $R=(T_D/T_2)^{1/2}$ (T_D is the time of spin diffusion across the skin-depth δ, and T_2 is the spin-relaxation time).

And conversely, when the intercalation front advances into the plate, the width of its intercalated part increases and, therefore, the frequency of collisions of GIC current carriers with these interfaces decreases. Therefore, at non-zero probability of spin reorientation of GIC current carriers during such collisions, the decrease of the total rate of spin relaxation of graphite current carriers (the graphite CESR linewidth) with the time of intercalation can be observed.

The increase of $A^*/B^*(\tau)$ dependence at the beginning of intercalation from ~1 until ~1.6 (Fig. 3) corresponds to a theoretical $A/B(l/\delta_c)$-dependence changing when increasing l/δ_c (Fig. 8). At the constant value of electrical conductivity along the c-axis of the forming GIC stage, this fact also points to the presence of the non-conductive barrier through the intercalation front and on its advance into sample.

Using the relation $(d^*)^2=2D_{int}\times\tau$ the experimental dependence $\Delta H(\tau)$ can be easily transformed into the dependence $\Delta H(a)$, where $a = l-2d^*$ is the thickness of the non-intercalated part of HOPG plate (Fig. 6). The latter dependence can be calculated theoretically as well, using the exdended Dyson expressions for the CESR in metals including the effects of surface spin relaxation [15].]. It is assumed in this theory that an electron colliding with the surface has a certain probability ε of spin reorientation, in addition to the steady probability $1/T_2$ (T_2 is the spin-relaxation time due to the collisions of current carriers with the imperfections in the sample volume) which exists for all electrons. In the general Dyson expressions for CESR line shape [15] the contribution of the surface spin relaxation effects to the CESR line shape is determined by the value of the term $Q=1/2G\times\theta$, where $G=3\varepsilon/4\Lambda$ (Λ is the mean free path of current carriers) and θ is the sample thickness. (The analysis of the mentioned Dyson expression has shown that at given sample thickness the CESR linewidth increases with G value. For $G\neq0$, the value of CESR linewidth tends to the infinity at $\theta\rightarrow0$). Obviously, if $\varepsilon\equiv\varepsilon_a$ is considered as an average value of probability of spin reorientation during collisions of graphite current carriers with the non-conductive phase boundary, then the extended Dyson expressions for the CESR in metals including the effects of surface spin relaxation of current carriers can be used for analysis of $\Delta H(a)$ dependence also. It is shown in Fig. 6, where the results of such analysis are presented, that the theoretical dependence of the graphite CESR linewidth, with non-zero values of G_a describes the experimental data well. The found value of G_a=2 cm^{-1} and the typical HOPG values of $\Lambda\equiv\Lambda_a=(0.4\div1.6)\times10^{-5}$ cm [22] correspond to $\varepsilon_a=(1\div4.2)\times10^{-5}$. For comparison, the surface spin reorientation probabilities of conduction electrons in Cu and Li bulk samples are equal to $\sim10^{-2}$ [23] and $\sim5\times10^{-6}$ [24], respectively.

The analysis of $\Delta H^*(\tau)$-dependence (Fig. 3) it is possible to execute on the same procedure, which above was used for the analysis of the $\Delta H(\tau)$-dependence (Fig. 6). The application of the specified technique of the analysis to the experimental $\Delta H^*(\tau)$-dependences (Fig.7) give the G_a^*-values: ~0.1 cm^{-1}. As we see, the value of G_a^* appreciably smaller than the value of G_a. The reason for this discreapency may be: 1) the strong surface spin-relaxation of the current carrier spins at their collisions with the GIC surface and/or 2) asymmetry of the magnetic properties of the intercalation front for current carriers "swooping" on this interface from the side of graphite and from the side of GIC.

The step-wise changes of the CESR signal intensity from the intercalated parts of the graphite plate in samples with $l >> \delta_c$ (Figs. 4 and 5) points to the repeated-batch introduction of intercalate into graphite. We asume that the reasons of such non-uniform introduction of intercalate may be the presence of threshold intercalation potential and the periodical impoverishing of intercalate molecule layers adsorbed on graphite. The absence of such step-wise changes of the CESR signal intensity in the graphite plate with $l\sim1.6\delta_c$ is indirect evidence for offered by us interpretation of this phenomenon.

5. CONCLUSION

Graphite intercalation by SbF_5 molecules have been studied by CESR technique in HOPG plates with widths being much more and comparable with the graphite skin-depth governed by ***c***-axis conductivity. As a result, the significant narrowing (broadening) of the GIC (graphite) CESR signal during transport of the intercalate through the initial graphite sample and the step-wise changes in the intensity of the intercalated graphite CESR signal on exposure time in SbF_5 atmosphere have been clearly detected. The narrowing (broadening) of GIC (graphite) CESR signal during the advance of the intercalation front into the initial graphite sample is explained by non-zero probability of spin reorientation during collisions of current carriers with the interface between the intercalated and the non-intercalated parts of the plate. The assumption is made that the reasons of step-wise introduction of intercalate are the presence of threshold intercalation potential and the periodical impoverishing of intercalate molecule layers adsorbed on graphite. Similar experimental and theoretical investigations of graphite intercalation by other intercalants are in progress

ACKNOWLEDGEMENTS

The authors are grateful to V.V. Sereda for help in experiments, to Drs. L.B. Nepomnyashchii (Scientific Research Centre for Graphite, Moscow) and A.K. Tsvetnikov for providing us with the HOPG and SbF_5, respectively. This work was supported by the Russian Foundation for Basic Research (grant # 00-03-32610).

References

[1] Dresselhaus MS, Dresselhaus G. Intercalation compounds of graphite. Adv. Phys. 1981; 30(2):139-326.

[2] Solin SA. The nature and structural properties of graphite intercalation compounds. Adv. Chem. Phys. 1982; 49:455-532.

[3] Clarke R, Uher C. High-pressure properties of graphite and its intercalation compounds. Adv. Phys. 1984; 33(3):469-566.

[4] Endo M, Enoki T, Suematsu H, Yamanaka, editors. Proceedings of the 10th International Simposium on Intercalation Compounds-ISIC 10 [special issue]. Mol. Cryst. and Liq. Cryst. 2000; 340.

[5] Solin SA, Zabel H. The physics of ternary graphite intercalation compounds. Adv. Phys. 1988; 37(2):87-254.

[6] Lagrange P, Herold A, Herold C. Why mono- or polylayered intercalated sheets in graphite-electron donors systems? Mol. Cryst. Liq. Cryst. 1998; 310:33-42.

[7] Davidov R, Milo O, Palchan I, Selig H. ESR study of graphite-fluorine and graphite-fluoride acceptor intercalation compounds. Synth. Met. 1983; 8:83-87.

[8] Palchan I, Davidov D, Zevin V, Polatsek G, Selig H. An in situ ESR study of the intercalation mechanisms: HOPG/fluorine and HOPG/HNO_3. Synth. Met. 1985; 12:413-418.

[9] Palchan I, Mustachi F, Davidov D, Selig H. ESR study of dulate intercalation compounds: C/F, C/K/F and C/Li/F. Synth. Met. 1984/85; 10:101-106.

[10] Nakajima M, Kawamura K, Tsuzuku T. ESR study of HNO_3 intercalation process of graphite. J. Phys. Soc. Jpn. 1988; 57(5):1572-1575.

[11] Ziatdinov AM, Tsvetnikov AK, Mishchenko NM, Sereda VV. In situ ESR studies of intercalation of SbF_5 molecules into highly oriented pyrolitic graphite. Mat. Sci. Forum (Intercalation Compounds - ISIC-6) 1992; 91-93:583-588.

[12] Ziatdinov AM, Mishchenko NM. In situ ESR study of the HNO_3-intercalate diffusion process in graphite intercalation compounds. J. Phys. Chem. Solids 1997; 58(7):1167-1172.

[13] Ziatdinov AM, Skrylnik PG. Graphite intercalation by nitric acid: conduction ESR and theoretical studies. Chem. Phys. 2000; 261(3):439-448.

[14] Vogel FL, Foley GMT, Zeller C, Falardeau ER, Gan J. High electrical conductivity in graphite intercalated with acid fluorides. Mater. Sci. and Engin. 1977; 31(2):261-266.

[15] Dyson FJ. Electron spin resonance absorption in metals. II. Theory of electron diffusion and the skin effect. Phys. Rev. 1955; 98(2):349-359.

[16] Kaplan JI. Application of the diffusion-modified Bloch equation to electron spin resonance in ordinary and ferromagnetic metals. Phys. Rev. 1959; 115(3):575-577.

[17] Feher G, Kip AF. Electron spin resonance absorption in metals. I. Experimental. Phys. Rev. 1955; 98(2):337-348.

[18] Kodera HJ. Dyson effect in the electron spin resonance of phosphorus doped silicon. Phys. Soc. Jpn. 1970; 28(1):89-98.

[19] Ziatdinov AM, Mishchenko NM. Electron spin resonance lineshape and kinetic parameters of the conduction electrons in highly anisotropic conductors: highly oriented pyrolitic graphite. Phys. Solid State 1994; 36(8):1283-1289.

[20] Zevin V, Suss JT. ESR in layer-substrate structures: The line shape and nondestructive contactless measurements of the layer conductivity. Phys. Rev. 1986; B34(10):7260-7270.

[21] Saint Jean M, McRae EP. Planar diffusion constant D_a in acceptor-graphite intercalation compounds. Phys. Rev. 1991; B43: 3969-3974.

[22] Spain IL. Electronic transport properties of graphite, carbons, and related materials. Walker PL, Throweer Jr and PA, editors. Chemistry and physics of carbon, vol 8, New York:Dekker, 1973:119-305.

[23] Walker MB. Surface relaxation and quasiparticle interactions in conduction-electron spin resonance. Phys. Rev. 1971; B3(1):30-41.

[24] Zhikharev VA, Kessel AR, Kharakhashian EG, Cherkasov FG, Svarts KK. Conduction Electrons spin echo in metals. Soviet Physics - JETP 1973; 64(4): 1356-1366.